Effects of Mechanical Drawing on Gas Transport in an Emulsion Acrylic Multipolymer

M. J. EL-HIBRI and D. R. PAUL, *Department of Chemical Engineering and Center for Polymer Research, The University of Texas, Austin, Texas 78712*

Synopsis

A study was conducted on the gas sorption and transport properties of a multiphase commercial acrylic polymer trade-named Korad ACV before and after subjecting the polymer to mechanical drawing operations. The Korad system is an emulsion-polymerized amorphous composite comprised of a glassy, predominantly PMMA matrix phase and a poly(butyl acrylate)-dispersed phase surrounded by a PMMA/PBA copolymer shell. Large increases (up to eightfold) in permeability P to several gases were observed upon drawing Korad. The observed changes in the permeability to He, Ar, N_2, and CH_4 on drawing were correlated with the draw ratio, drawing temperature, and molecular diameter of the gas penetrant. Most of the increase in permeability occurred at low draw ratios (1–2). The increases in P were most dramatic for drawing temperatures below or near the T_g of the matrix phase (about 90°C) and were quite small for drawing temperatures 30°C or more above the matrix T_g. The extent of the permeability increase also depended on the gas, being greatest for CH_4 and essentially imperceptible for He. The changes in permeability behavior were interpreted in terms of a morphological transformation in the phase of the drawn Korad, which causes the originally dispersed rubber particles to assume a more continuous character. The behavior of the composite was modeled by the Takayanagi and Nielson treatments of two-phase composite systems. Volumetric, thermal, mechanical, and viscoelastic properties were measured for the as-received and processed Korad films to elucidate physical changes in the drawn polymer.

INTRODUCTION

A number of published reports[1-5] demonstrate that molecular orientation of amorphous polymer films by mechanical drawing causes significant improvements in the gas barrier characteristics of the material, i.e., reductions in permeability and diffusion coefficients. Studies to date have been primarily restricted to single phase systems whereas for some applications knowledge of the transport performance of multiphase blends or composites is often necessary. This is because, in their end uses, many polymers contain additives such as rubber modifiers for toughening inherently brittle glassy plastics like poly(vinyl chloride), polystyrene, and poly(methyl methacrylate).

This paper reports the effects of mechanical drawing on the gas transport behavior of a multiphase amorphous polymer which is a rubber-modified commercial acrylic polymer trade-named Korad ACV prepared by a multistage emulsion polymerization process. The material was received as film (nominally 3 mils thick) made commercially via melt extrusion by Polymer Extruded Products.

As background to this work, the chemical and physical characteristics of the polymer are described, and the gas sorption and transport properties

CCC 0021-8995/86/082583-34$04.00

are examined for the as-received material. The effects of drawing on the transport properties of the polymer are then dealt with. Drawing was done at room temperature and over the range 70 to 130°C. The transport properties have been correlated with draw ratio, drawing temperature, and the molecular diameter of the penetrant gas. Physical characterization of the drawn films included density, thermal analysis, and static and dynamic mechanical measurements. The extent of orientation in the drawn samples was assessed from thermal shrinkage measurements. The study was primarily confined to uniaxial drawing; however, a few cases of biaxial drawing were also examined which suggest that for this system biaxial and uniaxial drawing have similar effects on transport behavior.

STRUCTURE OF KORAD ACV

Korad ACV is a fully amorphous acrylic polymer product produced by multistage emulsion polymerization. Rather thorough details of the process are given in a U.S. patent.[6] Briefly, the process can be described as consisting of the following steps. Initially, butyl acrylate (BA) is emulsion-polymerized in the presence of a small amount of 1,3-butylene glycol diacrylate, thus forming a crosslinked PBA rubber core. Following this, a second stage of polymerization is performed around the PBA particles. This involves copolymerizing a mixture of methyl methacrylate (MMA) and butyl acrylate, containing in the neighborhood of 60% MMA by weight. Third and fourth polymerization stages are then performed in a similar manner using feeds which contain predominantly MMA monomer. Typical compositions given in the patent for the third and fourth stages are 90/10 parts MMA/BA and 94/2/4 parts MMA/BA/MAA (methacrylic acid), respectively. The weight fraction of the rubbery polymer formed in the first polymerization stage is stated to be between 25 and 40% by weight for the products described in the patent. The remaining weight is divided almost equally among the three other stages. With the exception of one five-stage polymerization mentioned, all the products described were made by a four-stage process.

The idealized structure of the Korad emulsion polymerization particle is illustrated in Figure 1. The most important physical feature of this polymer is the existence of three distinct phases including a PBA crosslinked rubber phase, a copolymer phase, and a predominantly MMA polymer phase which will form the matrix when this material is melt-extruded to form a film. The intermediate copolymer phase separating the matrix from the PBA rubber particles is believed to act as a compatibilizing agent between the rubbery core and glassy matrix. The existence of the three phases has been confirmed by thermal analysis and dynamic mechanical testing described in a later section.

To obtain an estimate of the actual composition for Korad ACV, its mechanical properties were compared with those of the seven products described in the mentioned patent as shown in Table I. The tensile yield strength, percent elongation at break, and Young's modulus of the sample used in this study seem to fall closest to values corresponding to the product designated as "B." The composition of product B as described by the patent[6]
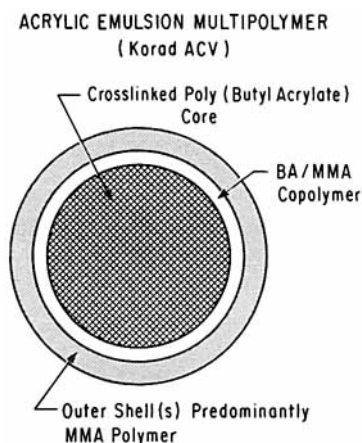
ACRYLIC EMULSION MULTIPOLYMER
(Korad ACV)

Fig. 1.   Idealized structure of a Korad emulsion polymerization particle.

is given in Table II. This polymer contains a MMA/BA weight ratio of about 54/46 and the PBA core phase constitutes about 35% of the total mass of the polymer. The MMA/BA content was also estimated by another approach based on measured volumetric properties. It is known that for blends and copolymers a linear volume additivity relationship adequately relates the density of the composite to the weight fractions and densities of its constituent components, in this case PBA and PMMA. This relation can be written as

$$\frac{1}{\rho} = \frac{W_1}{\rho_1} + \frac{W_2}{\rho_2} \tag{1}$$

Thus, using density data available for PBA[7] and PMMA[8] (1.09 and 1.18 g/cm^3, respectively) and the measured density for Korad ACV, the MMA weight fraction was computed to be 50%, which agrees reasonably well with the 54/46 ratio obtained from the mechanical property comparison. The product B composition can, therefore, be taken as a sufficient approximation for Korad ACV to allow modeling of the influence of mechanical drawing on transport behavior as described later.

TABLE I
Mechanical Properties[a] of Multistage Emulsion-Polymerized Acrylic Films[b]

Product	Modulus (psi) × 10^{-5}	Yield strength (psi)	Elong. at break (%)
Examples			
1 and 2	2.69	5170	51
A	2.08	4250	57.2
B	1.73	3760	69.1
C	1.22	3010	65.1
D	2.16	4685	48.8
E	2.19	4630	52.6
Korad ACV	1.47	4040	70

[a] Measured along extrusion machine direction.
[b] Examples 1 and 2 and products designated A, B, C, D, and E are described in Ref. 6.

TABLE II
Presumed Composition of Korad ACV (Product B in Patent)

Stage	Composition[a] (parts by weight)	Stage total
1	BA:BGDA = 35:0.35	35.35
2	BA:MMA = 8.7:13	21.7
3	BA:MMA = 2.2:19.5	21.7
4	BA:MMA:MAA = 0.4:21.3:1	22.7
Total[b]	BA:MMA = 46.65:53.8	101.45
Wt % (MMA/BA)	53.6% MMA, 46.4% BA	

[a] BA = butyl acrylate, BGDA = 1,3-butylene glycol diacrylate, MMA = methyl methacrylate, and MAA = methacrylic acid.

[b] BGDA and MAA parts have been incorporated into the BA and MMA totals, respectively.

EXPERIMENTAL

Korad films were drawn uniaxially at controlled temperatures using a procedure similar to that described earlier.[2] This was accomplished by a Table Model Instron mechanical tester fitted with an environmental chamber to allow a controlled environment from room temperature to 150°C. A strain rate of 100% min^{-1} was used throughout, and the actual draw ratio was measured from ink marks placed along the transverse direction prior to drawing. Some undrawn samples were heat-treated at the drawing temperature to give these films the same thermal history as the drawn material. Such films are designated as having a draw ratio of 1.0 (or 1.0X), as opposed to the "as-received" films which underwent no such heat treatment. The vast majority of drawn samples were of the uniaxial type; however, a few films were drawn in the biaxial mode using a T.M. Long tentering machine made available to us through the courtesy of Shell Development Co. Temperatures and strain rates were similar to those of the uniaxial drawing case, and the drawing was identical along the two mutually perpendicular directions within the plane of the film.

The physical state and behavior of as-received and processed Korad films were characterized using several techniques. Density was measured by a density gradient column using an aqueous calcium nitrate solution and factory calibrated density glass beads. Thermal behavior was characterized by differential scanning calorimetry (DSC) and dynamic mechanical testing (DMT). DSC measurements were performed on a Perkin-Elmer DSC-2 interfaced to a microprocessor for control and data acquisition. DSC data were normalized to a unit mass basis for easier comparison between different samples. DMT was done on a Rheovibron under the control of a computer automation and data acquisition system. The oscillation frequency was 110 Hz in all cases, and the temperature range covered was from −100 to 130°C.

The modulus, ultimate strength, and percent elongation at break were measured at ambient conditions along the machine direction for as-received and drawn Korad films using the Table Model Instron. The test specimens were rectangular strips 5/8 in. wide with a gauge length of 3 in. The crosshead speed was 0.5 in./min amounting to a strain rate of 16.7%/min. The reported mechanical property data are averages of those from several samples.

Thermal shrinkage measurements were taken on the drawn Korad samples by annealing the films at a given temperature for 10 min in the environmental chamber with no imposed stress. The shrinkage data were used to evaluate the extent and nature of orientation in the drawn Korad.

Equilibrium sorption of N_2, Ar, CH_4, and CO_2 in Korad was measured at 35°C and pressures from 0 to 25 atm using the pressure decay method. The stainless steel, dual-volume cell used allows accurate gas sorption determinations as described elsewhere.[9,10] Gas transport was measured for He, Ar, N_2, and CH_4 at pressures from 1 to 25 atm using the high pressure cell design and procedures described earlier.[9,11] The transport runs allowed measurement of both the steady-state permeability and the diffusion time lag. Because of its fluid rubbery nature, poly(butyl acrylate) required special preparation and handling procedures for the transport specimen which are described in a recent publication.[12] With the exception of the activation energy measurement runs, all gas transport experiments were conducted at 35°C. Also, unless otherwise specified, a constant pressure of 3 atm was used as the upstream boundary driving pressure p_2 for all transport runs. A nearly zero pressure boundary condition was maintained downstream from the membranes for all transport work. The pressure rise on the downstream side due to gas flow, p_1, never exceeded 10 mm Hg during the course of a transport run, which made p_1 negligible. All gases used had a purity of 99.7% or better except for CH_4, which was 99% pure.

RESULTS AND DISCUSSION

Sorption and Transport Properties of As-Received Korad ACV

In the glassy state, polymers sorb gases and vapors according to a mechanism which leads to a concentration–pressure isotherm relationship described by

$$C = k_D + \frac{C'_H bp}{1 + bp} \tag{2}$$

which is the sum of a Henry's law solubility contribution and a Langmuir type sorption term. Discussions dealing with the significance of the model and the parameters associated with it have been given elsewhere.[13-15] The values of k_D, C'_H, and b can be obtained by a nonlinear least squares analysis of the concentration–pressure data. Figure 2 depicts the sorption data for N_2, Ar, and CH_4 in Korad at 35°C. The model parameters extracted from the data are listed in Table III.

Given the heterogeneous nature of Korad ACV, the observed sorption levels represent a volume-fraction-based average corresponding to the separate phases present in the system. For a composite consisting of three distinct phases, the overall solubility k_c can be written as

$$k_c = \phi_1 k_1 + \phi_2 k_2 + \phi_3 k_3 \tag{3}$$

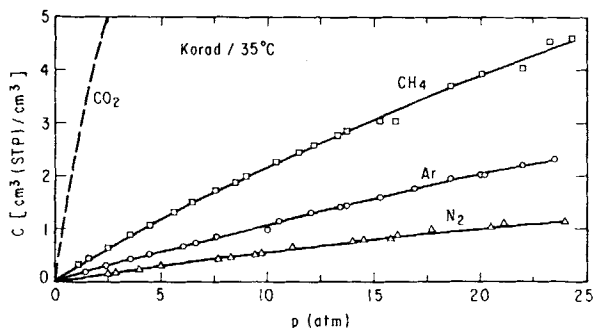where ϕ_1, ϕ_2, and ϕ_3 are the volume fractions of phases 1, 2, and 3, re-

Fig. 2. Sorption isotherms for N_2, Ar, and CH_4 in Korad at 35°C.

spectively, and k_1, k_2, and k_3 are the corresponding intrinsic solubility coefficients. For a miscible blend or a random copolymer of two components, on the other hand, the overall solubility k_b is well described by[16]

$$\ln k_b = \phi_1 \ln k_1 + \phi_2 \ln k_2 \qquad (4)$$

In the case of Korad ACV, two of the three phases present can be considered, to a first approximation, as pure homopolymers whereas the third is a copolymer. Thus, the overall solubility of the Korad composite is given by eq. (3), with the subscripts 1, 2, and 3 denoting the matrix, copolymer, and PBA phases, respectively. The k_2 for the copolymer must be obtained according to eq. (4),

$$\ln k_2 = \phi_1' \ln k_1 + \phi_3' \ln k_3 \qquad (5)$$

where ϕ_1' and ϕ_3' here represent the volume fractions of MMA and BA units within the copolymer phase. This leaves k_1 and k_3 as the only independent unknowns of eqs. (3) and (5). From knowledge of the overall Korad solubility coefficient k_c and the gas solubility data for PMMA available from Chiou and Paul,[17] one can estimate the solubility coefficients for various gases in PBA. This was done, and the results of these calculations are summarized in Table IV for N_2, Ar, and CH_4. PBA has a glass transition temperature T_g of about −50°C and, hence, is well within the rubbery state at 35°C. Thus, a Henry's law solubility coefficient is the only parameter needed to describe its sorption, as the Langmuir sorption contribution vanishes at T_g. It is worth noting that the sorption parameters in eq. (1) for different gases in

TABLE III
Dual Sorption Parameters[a] for N_2, Ar, CH_4, and CO_2 in Korad at 35°C

Gas	k_D	C_H'	b	$k_D + C_H'b$	k_a[b]
N_2	0.0385	0.493	0.0410	0.0587	0.568
Ar	0.0799	0.875	0.0433	0.1178	0.111
CH_4	0.1315	2.696	0.0449	0.2526	0.252
CO_2	1.432	3.803	0.3388	2.720	

[a] Units: k_D, k_a [=] [cm³(STP)/cm³ atm]; C_H'[=] [cm³(STP)/cm³] b[=] atm⁻¹.
[b] Obtained from time lag experiment at 3 atm.

TABLE IV
Henry's Law Gas Solubility Coefficients in PMMA and PBA at 35°C

Gas	k_D [cm³(STP)/cm³ atm]	
	PMMA[a]	PBA[b]
N_2	0.0737	0.0129
Ar	0.115	0.048
CH_4	0.182	0.0851

[a] Data from Chiou and Paul.[17]
[b] Estimated from Korad multiphase sorption calculations.

a given polymer have been shown to correlate with the Lennard–Jones potential well depth, ϵ/K, for the gas in the form of a linear semilogarithmic plot of the sorption parameters against ϵ/K.[2,12,17-22] This was found to be true also for Korad but the results are not shown here. The estimated Henry's Law constants for PBA listed in Table IV are also very well described by a linear correlation with respect to ϵ/K, which serves as a check on the consistency of these estimates.

Transport of He, Ar, N_2, and CH_4 in as-received Korad film was examined at 35°C and at pressures ranging from 1 to 25 atm. Permeability coefficients P for various gases are shown in Figure 3 plotted against the driving pressure p_2. Traditionally, for glassy polymers, the permeability for fixed gases is either completely independent of or shows a modest decline with p_2 in
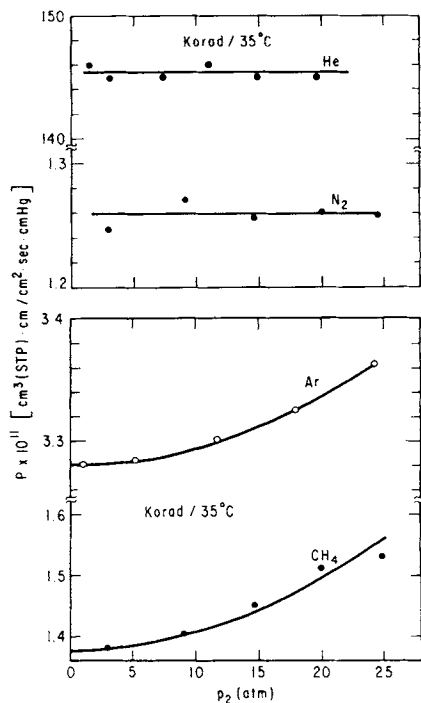

Fig. 3.   Permeability of Korad at 35°C to He, N_2, Ar, and CH_4 plotted against the driving pressure p_2.

accord with the dual-mobility permeation model described earlier.[23] However, it is noted for Ar and CH_4 in Korad that permeability increases with p_2 in the same fashion observed for CO_2 permeation in some glassy polymers such as PMMA and cellulose acetate[17,24] but to a much smaller extent. About 2.5 and 5% increases in P over the 25 atm pressure range were observed for Ar and CH_4, respectively. The permeabilities of He and N_2 are independent of pressure as evident in Figure 3. The time lags θ for Ar, N_2, and CH_4 plotted in Figure 4, as expected, show a small decline with p_2 consistent with observations for many other glassy polymers.

Effects of Drawing on the Transport Properties of Korad ACV

The effects of uniaxial drawing on the transport of various gases was first considered in terms of the draw ratio dependence of the permeability for a drawing temperature of 100°C. The highest T_g of the material, that of the matrix phase, is about 90°C, thus, by drawing at 100°C the entire composite was in the rubbery state. The maximum attainable draw ratio at this temperature was about 3, which is somewhat unusual since draw ratios as high as 5 have been reported for PMMA.[25] This is probably related to the multiphase nature of the polymer and the small starting thickness of the film in the present case. The permeabilities of He, Ar, N_2, and CH_4 in Korad are plotted against the draw ratio λ in Figure 5. The relative permeability, P/P_0, used to correlate the data denotes P for each gas normalized with respect to the permeability of that gas in the as-received film, P_0. Values for P_0 are given in Table V under the Korad ACV heading. Also listed in Table V are permeability values for PMMA and PBA. The PMMA values were excerpted from the work of Chiou and Paul,[17] while those for PBA were measured as part of this work at 35°C using the technique described above.

The P/P_0 points indicated at $\lambda = 1.0$ in Figure 5 correspond to a film which was not drawn but heat-treated at 100°C to acquire the same thermal
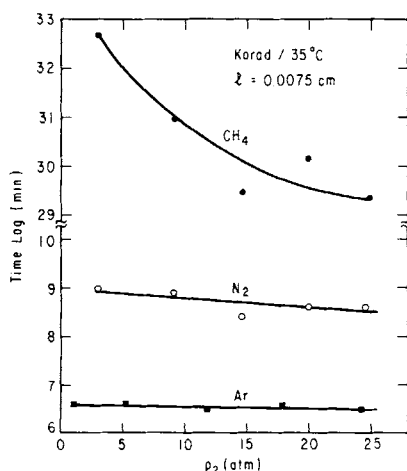

Fig. 4.   The diffusion time lags of Ar, N_2, and CH_4 transport in Korad at 35°C as a function of driving pressure p_2.
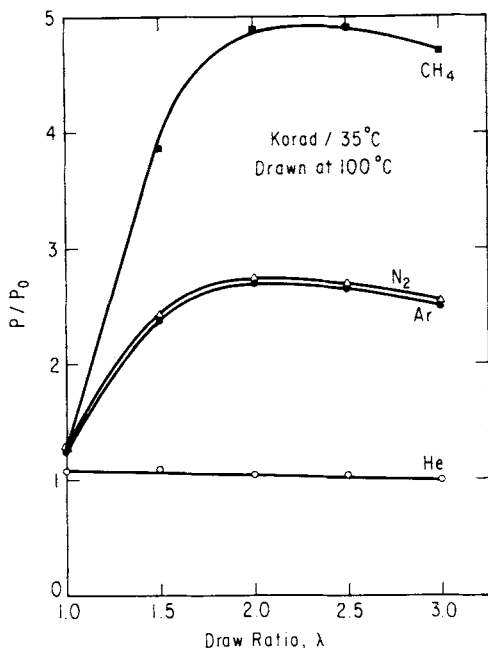
Fig. 5. P/P_0, the Korad permeability at 35°C relative to the as-received value plotted as function of draw ratio λ. Drawing temperature = 100°C.

history as that of the drawn samples. The as received film, thus, has P/P_0 = 1 for all gases according to this convention; however, heat treatment without drawing causes some changes in P such that $P/P_0 \neq 1$ in this case.

The results of Figure 5 reveal permeability changes in response to orientation which are quite dramatic and unexpected. The permeability of CH_4, for example, abruptly *increases* by about fivefold upon drawing Korad to a draw ratio of 2.0. A similar but less pronounced trend is observed for Ar and N_2 $(P/P_0 \sim 2.7$ at $\lambda = 2.0)$. On the other hand, the He permeability appeared to be rather insensitive to the physical changes brought about by drawing and, in fact, showed a decline of about 10% in P/P_0 at $\lambda = 3$ relative to that at $\lambda = 1$. The important feature in the shape of the curves for Ar, N_2, and CH_4 is the sharp initial rise in P/P_0 followed by a maximum value at about $\lambda = 2.0$. The sharp increases in P shown in Figure 5 are paralleled by reductions in selectivity of transport due to a molecular size dependence of the response as shown in Figure 6 for the gas pairs He/N_2

TABLE V
Permeabilities[a] of Various Gases in As-Received Korad ACV along with Those in PMMA and PBA

Gas	Korad ACV	PMMA[b]	PBA
He	1.46×10^{-9}	6.36×10^{-10}	1.07×10^{-8}
Ar	3.29×10^{-11}	2.13×10^{-12}	5.55×10^{-9}
N_2	1.27×10^{-11}	8.25×10^{-13}	1.97×10^{-9}
CH_4	1.33×10^{-11}	3.50×10^{-13}	1.10×10^{-8}

[a] Units: [cm³(STP) cm/cm² s cm Hg]
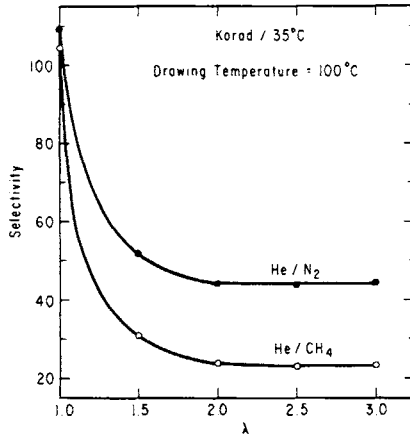[b] From Chiou and Paul.[17]

Fig. 6.   Korad permeation selectivity for He/N_2 and He/CH_4 at 35°C. Drawing temperature = 100°C.

and He/CH_4. The response of selectivity to drawing is almost a mirror image of that observed for permeability—drastic decreases in the initial stages of drawing followed by leveling off to a plateau value.

A first step in understanding the origin of the observed permeability behavior is to establish the relative importance of sorption and diffusion in the changes in P. This was done by comparing the solubilities of drawn and undrawn Korad films to N_2, Ar, CH_4, and CO_2. Unlike CO_2, the sorption levels for the other gases are quite low, which precluded an accurate comparison of sorption by the equilibrium method. Therefore, for these gases, the apparent solubility coefficients k_a derived from transient permeation measurements were compared instead. The apparent solubility coefficient is defined by

$$k_a = P/D_a \qquad (6)$$

where D_a, the apparent diffusion coefficient, is related to the time lag θ and membrane thickness l by

$$D_a = l^2/6\theta \qquad (7)$$
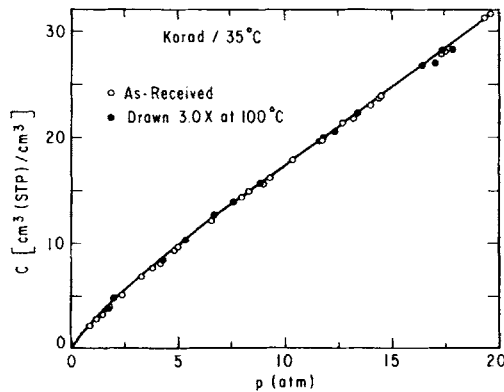
Fig. 7.   The CO_2 sorption isotherms at 35°C for the as-received (○) Korad and a film drawn to $\lambda = 3.0$ at 100°C (●).
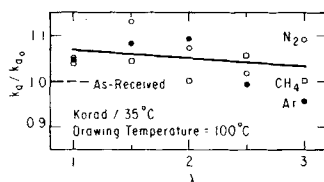
Fig. 8. Apparent solubility k_a of N_2, Ar, and CH_4 in Korad at 35°C relative to the as-received (- - -) value k_{a0} vs. draw ratio λ. Drawing temperature = 100°C.

The results of the sorption comparisons are shown in Figures 7 and 8 for CO_2 and the other gases, respectively. The results in both figures demonstrate conclusively the absence of any significant effect of drawing on solubility. The drawn Korad film used to obtain the CO_2 isotherm shrank by about 10% during exposure to high pressure CO_2. The observed scatter in the transient solubility data of Figure 8 is largely due to errors in measuring the time lags, which were rather short for the thin drawn films. On the scale observed here, however, it can be safely judged that the changes in P are almost exclusively attributable to changes in the diffusion coefficient for the system.

Molecular orientation in amorphous polymers is commonly examined by measuring the birefringence using standard interferometric devices. The applicability of this technique, however, hinges on whether or not the backbone of the polymer chain possesses a significant difference in intrinsic electronic polarizabilities in the directions along and normal to the polymer chain. Since this is not the case, generally, for the acrylic family of polymers, and since the film thicknesses involved were very small, birefringence changes were very small and could not be measured. As an alternative, thermal shrinkage of drawn films was used to give a semiquantitative measure of the orientation state in the films. A uniform period of 10 min at 100°C was used to shrink drawn samples. The results are presented in Figure 9 in two different ways as a function of initial draw ratio λ. Here, L_0 refers to the sample length prior to drawing, L is the length after drawing, and L_s is the length after shrinkage. Percent recovery is then defined as $100(L-L_s)/(L-L_0)$. The data indicate that a substantial amount ($\sim$70%) of the strain induced by drawing at 100°C is recoverable and, thus, manifests itself as frozen-in molecular orientation in the specimen prior to thermal annealing again at 100°C. The absolute strain frozen-in increases in direct proportion to λ as indicated by the line representing $\lambda - \lambda_s$ plotted in Figure 9.
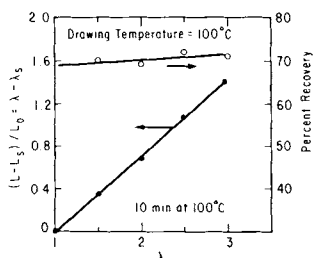

Fig. 9. Thermal shrinkage showing the percentage recovery (upper curve) and extent of recovery (lower curve) in Korad films as function of draw ratio. Films drawn at 100°C.

Effect of Drawing Temperature

Korad films were drawn to $\lambda = 2.0$ at temperatures ranging from 70 to 130°C, and physical characterization of these samples was performed to monitor changes in the state of the polymer. Permeability data are reported for drawn Korad ($\lambda = 2.0$) as a function of drawing temperatures in Figure 10. This plot reveals several facts about the role of the drawing temperature. The increase in P for Ar, N_2, and CH_4 becomes more pronounced as the drawing temperature is lowered, reaching a plateau at about 70°C. P/P_0 values were also obtained for a sample that was drawn at room temperature to its natural draw ratio of 1.5X. The data of this film for the various gases showed about half the magnitude of P/P_0 increases noted for the 2.0X sample drawn at 70°C. This leads us to believe that the effect of drawing below 70°C on P is essentially independent of drawing temperature, at least down to about 25°C, as implied by the low temperature plateau of Figure 10. For N_2 and Ar the P/P_0 values are so similar that these data can be represented by a single curve in Figure 10. In the high temperature region, the P/P_0 response tapers off asymptotically, reaching a low plateau only slightly above the level for the undrawn Korad. The narrow range of temperatures slightly above the T_g of the PMMA matrix (95–110°C) marks a rather abrupt transition region between the high temperature and the low temperature drawing regimes characterized by the plateaus described. For He, drawing temperature does not appear to have any influence as its permeability remained essentially unchanged from that of the as-received film. Values of P/P_0 for film drawn biaxially to 1.4X $\times$ 1.4X are indicated on Figure 10 by the open points, which lie very close to those of the uniaxially drawn film. Thus, the drawing temperature seems to be the single most important factor governing the transport response of this material. The level of strain is important only in the low strain region ($\lambda = 1.0$–2.0), as the permeability varies only slightly for higher strains.

To establish the effect of drawing temperature on the state of orientation for drawn Korad films, a plot of thermal shrinkage (Fig. 11) was generated for samples drawn over the same temperature range. The percent recovery shows a decline with drawing temperature, in general agreement with the permeability behavior of Figure 10. In Figure 12, data for similar shrinkage
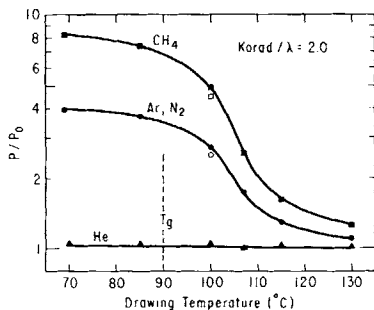

Fig. 10. Relative permeability of drawn Korad at 35°C vs. drawing temperature. Solid points designate uniaxial drawing to $\lambda = 2.0$; open points designate equal biaxial drawing to 1.4X $\times$ 1.4X = 2.0.
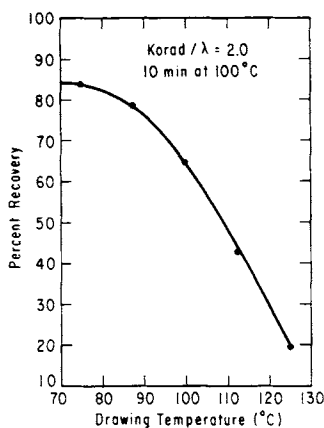
Fig. 11.   Percent recovery of Korad films drawn to λ = 2 vs. drawing temperature.

measurements are shown for samples drawn at 70, 100, and 130°C but allowed to shrink for 10 min at different temperatures in the range from 70 to 130°C. The results demonstrate that the shrinkage temperature strongly affects the observed level of recovery, particularly as temperatures in the range of 110°C are traversed, where an abrupt increase in the percent recovery is observed. The fact that the percent recovery exceeded 100% at high shrinkage temperature probably reflects a low level of initial orientation in the as-received film which cannot relax under less stringent conditions.

The penetrant molecular size dependence of the permeability increase on drawing is depicted in Figure 13 for two drawing temperatures (70 and 100°C). The penetrant dimension used to correlate the data is the Lennard–Jones mean molecular diameter derived from viscosity measurements,[26] and the straight lines drawn are based on the spherical penetrants: He, Ar, and CH_4. As seen later, this correlation stems from the composite nature of Korad and the strong effect of gas diameter on the relative permeabilities of the glassy and rubbery phases.

The apparent solubilities for Ar, N_2, and CH_4 were determined at different drawing temperatures to ascertain whether there is any change in
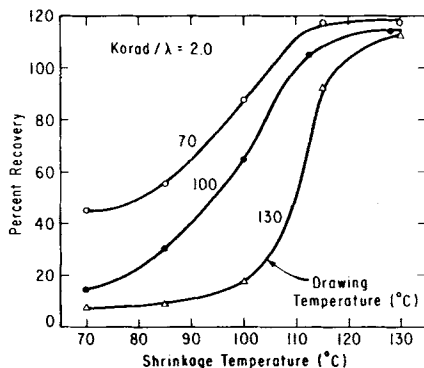

Fig. 12.   Percent recovery vs. shrinkage temperature for Korad films drawn to λ = 2.
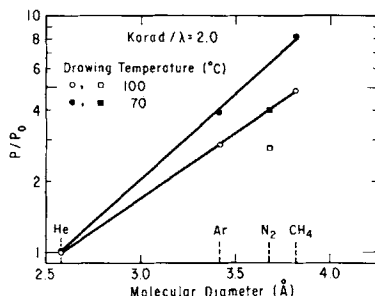
Fig. 13. Relative permeability at 35°C vs. Lennard–Jones penetrant molecular diameter for Korad drawn to $\lambda = 2$ at two drawing temperatures (°C): (○, □) 100; (●, ■) 70.

k_a with drawing temperature. The results are shown in Figure 14. Given the degree of scatter in the data, the average value of the Korad apparent solubilities $k_{a,av}$ was taken as the normalization parameter here instead of the as-received value k_{a0}. It is evident from the data that no particular trend is followed with temperature, and hence the solubility is, again, not a significant contributor to the permeability increases caused by drawing.

Figure 15 shows the density of films drawn to $\lambda = 2.0$ as a function of the drawing temperature. The density of drawn films does not vary with drawing temperature and is the same as the undrawn material. The fact that density remains unchanged by drawing rules out the possibility of craze formation or significant free volume changes on drawing. Thus, the drastic increases in permeability cannot be interpreted in terms of such processes.

Next, the effect of the temperature of the permeation measurement was examined. In Figures 16 and 17, Arrhenius plots for the permeabilities of He, N_2, Ar, and CH_4 are depicted over the temperature range from 35 to 60°C. This is done for the as-received sample and a sample drawn at 100°C ($\lambda = 2.0$). Since the permeability behavior is completely analogous to that of the diffusion coefficient, no separate plots are shown for the latter. Instead, the similar Arrhenius dependence for the apparent solubilities of N_2, Ar, and CH_4, which are unaffected by orientation, is shown in Figure 18. The permeability data of Figures 16 and 17 were used together with the solubility plot of Figure 18 to calculate the Arrhenius parameters for the diffusion coefficient. By this calculation, it was tacitly assumed that solubility is unaffected by drawing regardless of the experimental temperature. The Arrhenius parameters thus derived from the above data are listed in Table VI. Because of the composite nature of Korad, these parameters do not characterize a single, simple molecular process but are useful for a
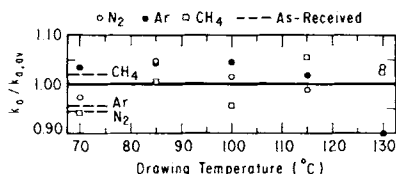

Fig. 14. Apparent Korad solubilities for various gases at 35°C normalized to average value $k_{a,av}$ vs. drawing temperature ($\lambda = 2.0$): (○) N_2; (●) Ar; (□) CH_4; (---) as-received.
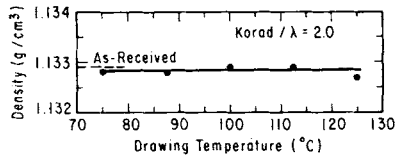
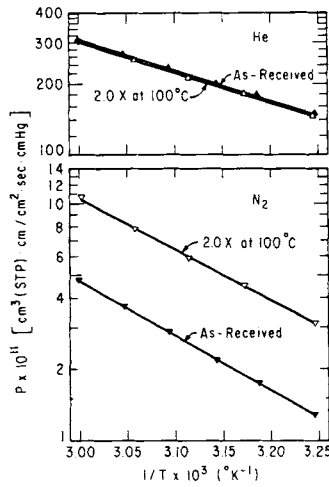Fig. 15.   Density of Korad films drawn to λ = 2.0 vs. drawing temperature.

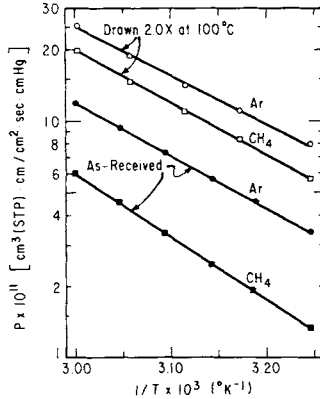Fig. 16.   Arrhenius plots of as-received and drawn (λ = 2.0) Korad permeabilities to He and N_2.

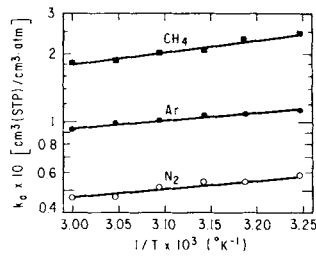Fig. 17.   Arrhenius plots of as-received and drawn (λ = 2.0) Korad permeabilities to Ar and CH_4.

Fig. 18.   Arrhenius plots of N_2, Ar, and CH_4 apparent solubility data in as-received Korad.

TABLE VI
Arrhenius Parameters[a] for Gas Transport in As-Received and Drawn Korad Film

Gas	Sample	$E_p{}^a$	P_0	E_D	D_0
He	As received	5.794	1.926×10^{-5}	—	—
	2.0X at 100°C	5.967	2.476×10^{-5}	—	—
Ar	As received	10.018	4.356×10^{-4}	11.562	3.615
	2.0X at 100°C	9.391	3.602×10^{-4}	10.937	2.993
N_2	As received	10.523	3.742×10^{-4}	12.421	10.761
	2.0X at 100°C	9.958	3.640×10^{-4}	11.857	10.483
CH_4	As received	12.023	4.56×10^{-3}	14.479	78.234
	2.0X at 100°C	10.058	7.855×10^{-4}	12.513	13.449

[a] Units: E_p, $E_D[=]$ kcal/mol; $P_0[=]$ cm^3(STP) cm/cm^2 s cm Hg; $D_0[=]$ cm^2/s.

phenomenological description of the effect of temperature on the behavior of this system.

Effects of Drawing on Morphology of Korad

Before proceeding with the model interpretations which follow, it is useful to consider the empirical presentation of these transport results shown in Figure 19. Here, the permeability of a given gas in the Korad composite has been normalized by the permeability of that gas in PMMA and plotted versus the ratio of the permeabilities of that gas in PBA and PMMA. The values of P_{PBA} and P_{PMMA} used in these calculations were taken from Table V. The ratio P_{PBA}/P_{PMMA} varies enormously with the size of the gas molecule as may be seen by the identification of the gases shown on the abscissa in Figure 19. The important point made by this plot is that it calls attention to the large differences in permeation rates through the rubbery and glassy parts of the Korad composite and provides a basis for understanding the influence gas type has on the response to drawing based on the greater P_{PBA}/P_{PMMA} ratio the larger the gas molecule.

The firgure shows data for undrawn ($\lambda = 1.0$) as well as drawn Korad samples. For the undrawn material P_{Korad}/P_{PMMA} increases steadily with the increase in P_{PBA}/P_{PMMA}, thus reflecting the contribution of the dispersed PBA phase to the permeability of the Korad system. Upon drawing, the same general relationship between P_{Korad} and P_{PBA} is maintained, but the normalized P values of Korad become progressively more pronounced with increasing P_{PBA}. Thus, the P_{Korad} values reflect a PBA contribution which
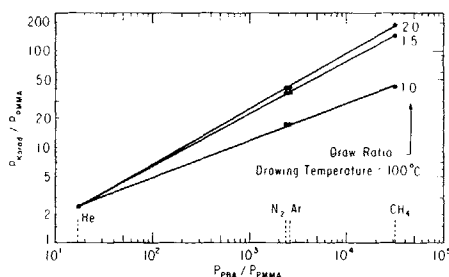

Fig. 19. Korad permeability at 35°C plotted against PBA permeability for various gases. All permeabilites are normalized with respect to PMMA permeability values.

becomes enhanced on drawing, and, because the ratio P_{PBA}/P_{PMMA} is much higher for the larger penetrants, the enhanced PBA contribution is translated into higher permeabilities for such gases. The same phenomenon underlies the drastic reductions in selectivity upon drawing (shown in Fig. 6) and agrees with the physical interpretations proposed in the following.

To explain the dramatic increases observed in P and D upon low-temperature drawing of Korad, it is necessary to analyze the morphological changes in the phase structure of the system. Such morphological changes must account for most of the observed transport property alterations, as the overall volume of the polymer does not show any significant increase with drawing. This section attempts to model the influence of the drawing process (restricted here to the uniaxial case) on the morphology of the Korad material and to examine the gas transport behavior that would be anticipated from given structural changes. The transport behavior predicted from the model calculations for the composite in different configurations is then compared with the experimental findings.

On a microscopic level, the Korad film can be visualized in terms of a matrix phase, consisting of predominantly PMMA polymer, in which an array of uniformly distributed rubber particles are dispersed. This morphology is depicted schematically in Figure 20(a). Gas transport through such a heterogeneous medium has been described by a multitude of mathematical models. For the purposes of this investigation, however, a quantitative description of the transport behavior based on the approach of Takayanagi for multiphase media[27-30] is informative. This approach has been conventionally used to model mechanical properties of composite systems, but it can be adequately employed here since the mechanical and the transport problems are mathematically similar.

The Takayanagi treatment involves the approximation that the array of spheres representing the dispersed phase in Figure 20(a) can be regarded as a regular array of cubes as shown in Figure 20(b). Conversion into this rectilinear geometry facilitates the computational aspects of the mathematical treatment which assumes all transport is unidirectional. Consequently, the morphology of Figure 20(b) is also equivalent to that where the matrix and the dispersed phases are regarded as two distinct bulk media having the geometry of Figure 20(c). The central morphological feature characteristic of a, b, and c in Figure 20 is that the matrix constitutes the continuous phase traversing the composite through all sides, whereas the dispersed phase, represented by the shaded areas, is embedded within it, thereby allowing the matrix phase to have the dominant contribution to the overall permeability of the system.
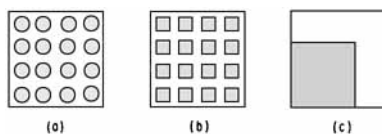

Fig. 20.   Schematic model of Korad morphology showing the dispersed phase (shaded areas) based on a spherical array of particles (a), and according to the Takayanagi treatment (b) and (c).
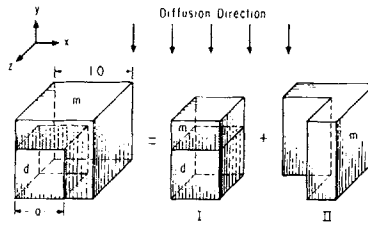
Fig. 21.   Three-dimensional Takayanagi representation of Korad composite comprised of a matrix phase m and a dispersed phase d. The system is also shown broken into its constituent parallel diffusional resistance components, I and II.

The Takayanagi model for Figure 20(c) is illustrated in Figure 21 on the left side in three-dimensional form. The entire composite is represented as a cube of unit volume. The matrix is designated on the cube by m. The dispersed phase, designated by d, is represented by the small cube of edge length a lying at the front left-hand corner of the system. According to Figure 21, then, the volume fraction of the dispersed phase, ϕ_d, is given by $\phi_d = a^3$ or $a = \phi_d^{1/3}$. Gas transport in the Korad composite medium can then be analyzed by breaking the system into its basic parallel and series diffusional components. This is illustrated in Figures 21 and 22. The transport medium defined on the left in Figure 21 is shown as the sum of two components. The first is a rectangular parallelepiped comprised of the dispersed phase and the portion of the matrix phase which lies above it along the y-projection of the xz plane of the dispersed phase; and the second component is formed by the remainder of the composite consisting exclusively of matrix material. The overall diffusive gas flow through the composite is the sum of the contributions corresponding to these two components which constitute a parallel flow arrangement. This arrangement is also depicted in the schematic diagram of Figure 22 in the form of parallel and series elements of the composite diffusional resistances characteristic of the system under consideration. The diffusion resistance combination corresponds to the two elements I and II shown in Figure 21. It consists of two parallel resistance branches, one of which (I) is comprised of a two-element series arrangement.
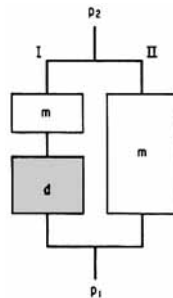
Fig. 22.   Diffusional resistance combination in Takayanagi system, m and d designates matrix and dispersed phases, respectively. p_1 and p_2 represent pressures at lower and upper system boundary, creating diffusional driving force.

Permeation Model for Undrawn Korad

The model described for Korad in connection with Figures 20–22 is used below to develop an expression for the permeability of the undrawn Korad, P_1, in terms of P_m and P_d, the matrix and dispersed phase permeabilities, respectively, and ϕ_d, the volume fraction of the dispersed phase. All the variables and notation employed in the derivation below are as defined in Figures 20–22.

In reference to Figure 22 the diffusive gas flow across the entire composite is the sum of the flows corresponding to components I and II. Diffusive flow for a given section i is defined as

$$\text{flow} = P_i A_i / l_i \tag{8}$$

where P_i is the permeability of that section and A_i and l_i are the diffusion area and the section thickness, respectively. For a section consisting of two or more elements stacked in series, the expression describing the effective permeability of that section can be obtained from the well-known series model

$$\frac{P_s A_s}{l_s} = \left[\frac{l_1}{P_1 A_s} + \frac{l_2}{P_2 A_s} + \frac{l_3}{P_3 A_s} + \cdots \right]^{-1} \tag{9}$$

where the subscript s refers to the series composite and $1, 2, 3, \ldots$ refer to the individual components. With the above concepts in mind, one can proceed to write expressions for the diffusive flows in components I and II as follows:

$$\text{I:} \quad \frac{P_I a^2}{l_I} = \left[\frac{a}{P_d a^2} + \frac{1 - a}{P_m a^2} \right]^{-1} \tag{10}$$

$$\text{II:} \quad \frac{P_{II}(1 - a^2)}{l_{II}} = P_m (1 - a^2) \tag{11}$$

$$\text{Total (I + II):} \quad P_1 = \left[\frac{a}{P_d a^2} + \frac{1 - a}{P_m a^2} \right]^{-1} + P_m (1 - a^2) \tag{12}$$

which, upon substituting $\phi_d^{1/3}$ for a gives the expression

$$P_1 = \phi_d^{2/3} \left[\frac{\phi_d^{1/3}}{P_d} + \frac{1 - \phi_d^{1/3}}{P_m} \right]^{-1} + P_m (1 - \phi_d^{2/3}) \tag{13}$$

Equation (13) thus describes the permeability of Korad in the undrawn state. The equation is somewhat oversimplified in that it treats the PBA phase and its encasing (BA/MMA) copolymer shell as a single phase. The model is adequate, however, considering the primary objective is to examine the influence of drawing on the transport properties which would manifest themselves through changes in eq. (13).

Permeability of Drawn Korad—Model 1

The following model is a first attempt to analyze the observed permeability increases on the basis of geometrical changes occuring on drawing. It is based on the assumption that the deformation introduced into the matrix phase by drawing is accompanied by an equivalent deformation in the dispersed rubber particles. This process is illustrated in the upper frame of Figure 23 depicting both the array of rubber particles and the system according to the Takayanagi approach. It must be kept in mind that the schematic depiction of Figure 23 is for a case where ϕ_d is about 0.25, whereas the actual ϕ_d for Korad is 0.5–0.6. The length of the model system shown in Figure 21 is increased on drawing by a factor of λ, whereas the width and thickness dimensions contract by a factor of $1/\sqrt{\lambda}$ each, since no volume changes occur on drawing. Thus, the new system dimensions after drawing become λ for the length and $1/\sqrt{\lambda}$ for the width and thickness. For the dispersed phase, the corresponding dimensions are λa and $a/\sqrt{\lambda}$. The permeability of the drawn composite, P_λ, is evaluated following exactly the derivation of eq. (13). Thus, adopting model 1 for the drawn film the diffusive flows are

$$\text{I:} \quad \frac{P_I(a/\sqrt{\lambda})\lambda}{1/\sqrt{\lambda}} = \left[\frac{a/\sqrt{\lambda}}{P_d(a\sqrt{\lambda})a\lambda} + \frac{(1-a)/\sqrt{\lambda}}{P_m(a/\sqrt{\lambda})a\lambda} \right]^{-1}$$

$$= \lambda \left[\frac{a}{P_d a^2} + \frac{(1-a)}{P_m a^2} \right]^{-1} \tag{14}$$

$$\text{II:} \quad \frac{P_{II}[(1/\sqrt{\lambda})\lambda - (a/\sqrt{\lambda})\lambda]}{1/\sqrt{\lambda}} = P_m(1-a^2)\lambda \tag{15}$$

Total (I + II): $\dfrac{P_\lambda(1/\sqrt{\lambda})\lambda}{1/\sqrt{\lambda}} = P_\lambda\lambda$

$$= \lambda \left[\frac{a}{P_d a^2} + \frac{(1-a)}{P_m a^2} \right]^{-1} + P_m\lambda(1-a^2) \tag{16}$$
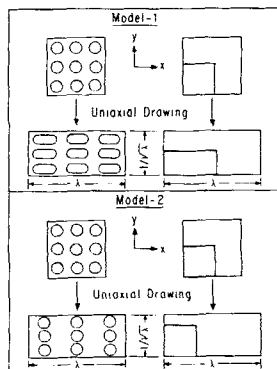

Fig. 23.   Two Korad deformation mechanisms. Model 1: m and d phases deform in uniform manner. Model 2: only m phase deforms.

Hence

$$P_\lambda = \phi_d^{2/3} \left[\frac{\phi_d^{1/3}}{P_d} + \frac{1 - \phi_d^{1/3}}{P_m} \right]^{-1} + P_m(1 - \phi_d^{2/3}) \qquad (17)$$

·Equation (17) is identical to eq. (13) above, therefore, the morphological change produced by drawing according to model 1 in Figure 23 cannot be expected to yield any significant change in the transport behavior as demonstrated from the P_λ expression, which corresponds to this case. In fact, since the transport properties P and D for the matrix are expected to decline upon orientation, as shown to be the case for numerous glassy polymers,[1-5] the Korad permeability would be expected to show a noticeable decline based on these purely geometrical considerations, assuming no interactions between the rubbery elements in the oriented state. However, as will be shown subsequently, the observed increases in P cannot be explained except on the basis of such a morphological alteration, which can occur quite readily when the volume fraction for the dispersed phase is as high as it is for the Korad polymer.

Permeability of Drawn Korad—Model 2

The second deformation scheme considered in connection with the drawing of Korad is one in which the matrix phase deforms with the applied strain but the dispersed rubber phase does not. This situation is depicted in the lower half of Figure 23. Such a mechanism, while not affecting the shape of the dispersed particles, reduces the separation distance between neighboring particles along the direction normal to the plane of the film (the diffusion direction) and increases this separation along the machine direction. In terms of the equivalent Takayanagi system this translates into an expansion in the diffusion area of component II (Figs. 21 and 22) at the expense of a reduced thickness for the matrix phase in component I. Such morphological changes strongly affect the overall permeability behavior of the composite as the following analysis demonstrates.

According to model 2, the cube representing the entire composite in Figure 21 is transformed into a parallelepiped of dimensions λ, $1/\sqrt{\lambda}$, and $1/\sqrt{\lambda}$ as for model 1. The original shape of the dispersed phase remains unchanged, however. The system permeability in the drawn state, P_λ, can again be obtained for this case using the approach employed twice above. The diffusive flows in the individual components I and II and the overall system are as follows:

$$\text{I:} \quad \frac{P_\text{I} a^2}{1/\sqrt{\lambda}} = \left[\frac{a}{P_d a^2} + \frac{(1/\sqrt{\lambda}) - a}{P_m a^2} \right]^{-1} \qquad (18)$$

$$\text{II:} \quad \frac{P_\text{II}[(1/\sqrt{\lambda})\lambda - a^2]}{1/\sqrt{\lambda}} = P_m(\lambda - a^2\sqrt{\lambda}) \qquad (19)$$

Total (I + II): $\dfrac{P_\lambda (1/\sqrt{\lambda})\lambda}{1/\sqrt{\lambda}}$

$$= \left[\frac{a}{P_d a^2} + \frac{(1/\sqrt{\lambda}) - a}{P_m a^2}\right]^{-1} + P_m(\lambda - a^2\sqrt{\lambda}) \quad (20)$$

Therefore, P_λ reduces to

$$P_\lambda = \frac{\phi_d^{2/3}}{\lambda}\left[\frac{\phi_d^{1/3}}{P_d} + \frac{1/\sqrt{\lambda} - \phi_d^{1/3}}{P_m}\right]^{-1} + P_m\left(1 - \frac{\phi_d^{2/3}}{\sqrt{\lambda}}\right) \quad (21)$$

and thus the ratio P_λ/P_1 is given by

$$\begin{aligned}
\frac{P_\lambda}{P_1} = &\left[P_m\left(1 - \frac{\phi_d^{2/3}}{\sqrt{\lambda}}\right) + \frac{\phi_d^{2/3}}{\lambda}\left(\frac{\phi_d^{1/3}}{P_d} + \frac{1/\sqrt{\lambda} - \phi_d^{1/3}}{P_m}\right)^{-1}\right] \\
&\times \left[P_m(1 - \phi_d^{2/3}) + \phi_d^{2/3}\left(\frac{\phi_d^{1/3}}{P_d} + \frac{1 - \phi_d^{1/3}}{P_m}\right)^{-1}\right]^{-1} \quad (22)
\end{aligned}$$

The deformation model 2 described above is not the kind of behavior that one would normally expect from multiphase polymers like Korad and all works referred to in the literature dealing with mechanical and rheological behavior of rubber modified polymers seem to support model 1 over model 2. However, the latter has been considered here simply to explore the permeation behavior for such a possibility and to compare with the permeation behavior observed experimentally. This model is also based on the assumption that no rubbery interparticle contact whatsoever occurs on drawing (i.e., the dispersed phase particles are non-interacting).

From examining eq. (22) it is clear that P_λ/P_1, the relative permeability according to the model, is a function of the four parameters P_m, P_d, ϕ_d, and λ. For the case of Korad, ϕ_d has been taken as 0.584. This choice is based on the composition given in Table II for product B, which is similar to that of the product used in this work. The material of the dispersed (d) phase in the model calculations is taken to be that produced in the first and second polymerization stages, i.e., the PBA and the BA/MMA copolymer. The model results have proven to be relatively insensitive to moderate changes in ϕ_d. The values P_m and P_d are shown in Table VII, and are themselves computed from the intrinsic PMMA and PBA permeabilities using the Takayanagi model and the model for random copolymer permeability.[16] The relative permeabilities of He, Ar, N_2, and CH_4 are shown in Figure 24 as a function of λ over the λ range of 1 to 2. The reason that the P_λ/P_1 curves do not extend for the different gases beyond certain λ values is that eq. (22) cannot yield a physically meaningful permeability value when the quantity $(1/\sqrt{\lambda} - \phi_d^{1/3})$ becomes negative. In any case, the model behavior shown in the bottom part of Figure 23 seems to depart greatly from the relative permeability behavior actually observed both in the nature and magnitude of the changes predicted. For example, the curves of P_λ/P_1

TABLE VII
P_m and P_d, the Permeabilities of the Korad Continuous and Dispersed Phases, Respectively, Estimated from P Values for PMMA and PBA Using Standard Methods for Multicomponent Systems

Gas	$P_m{}^a$	$P_d{}^a$	P_d/P_m
He	6.92×10^{-10}	5.48×10^{-9}	7.9
Ar	2.69×10^{-12}	2.93×10^{-10}	108.9
N$_2$	1.04×10^{-12}	1.09×10^{-10}	104.8
CH$_4$	4.77×10^{-13}	1.44×10^{-10}	301.9

^{a} Units: same as for Table V.

begin with a small slope but then rapidly swing upward increasing many-fold over very small intervals of λ. The sizeable increase predicted in the He permeability also contradicts the experimental results. Thus, model 2 has to be rejected as a plausible explanation for the transport behavior in the drawn polymer.

In model 2 the permeability is predicted to increase on drawing because this reduces the relative separation of the rubber particles which, depending on gas type, are much more permeable than the matrix material separating them, whereas this relative separation does not change on drawing in model 1. However, in the limit

$$1/\sqrt{\lambda} - \phi_d^{1/3} = 0 \tag{23}$$

or when $\lambda = 1/\phi_d^{2/3}$ in terms of the Takayanagi geometrical approximation for model 2, these particles touch completely. Further drawing is not physically meaningful in the context of this approximation. At this limit, the composite becomes a perfect parallel arrangement of the m and d phases, and eq. (14) reduces to

$$P_\lambda = \phi_d P_d + \phi_m P_m \tag{24}$$

which is the expected result for this phase configuration. At this point, P_λ becomes more comparable to P_d than P_m as the former is much larger than the latter for the larger gases, and this is why Figure 24 shows a rapid
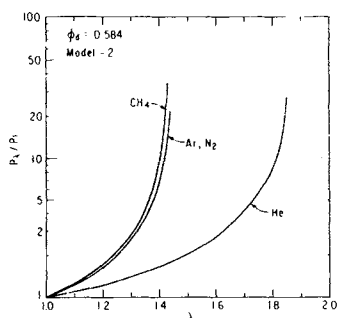

Fig. 24. P_λ/P_1, permeability of drawn Korad relative to undrawn value vs. λ as predicted by model 2.

upswing whose rate depends on gas type as λ approaches $1/\phi_d^{2/3}$. Physically, this abrupt conversion to a parallel morphology cannot occur since the particles are not rectangular, and thus it is an artifact of the Takayanagi approximation. Instead, the originally spherical particles may initially touch at a point and with higher stresses the area of contact (or interaction) between particles can increase as the particles deform at the point of contact, progressively increasing the effective connectivity or degree of parallel nature of this phase.

Thus, we feel that the actual morphological change occurring on drawing is probably a combination of the modes described in models 1 and 2 with the additional feature of particle touching or interaction creating a degree of more permeable paths, depending on the deformation of the particles as they touch, which will depend on the stresses pressing them together and the degree of axial deformation of these particles during drawing. This is a complex process which would be difficult to model in a completely deterministic way. However, the analysis given in the next section attempts to give a framework for considering the present results.

Permeability of Drawn Korad—Model 3

This last model treatment of the Korad orientation behavior is based on the deformation described above and considers a morphological transition of the rubbery component from being a strictly dispersed phase into a phase possessing both dispersed and continuous character. This transformation can be represented in terms of a model possessing two continuous phases akin to that proposed by Nielson.[31] The model is depicted in Figure 25, where the original dispersed phase volume fraction ϕ_d is divided into parallel and series components designated by the subscripts p and s, respectively. An equivalent three-dimensional system model is shown in Figure 25, where the composite is again viewed as a cube of unit volume with parallel and series components of both the d and m phases with respect to the diffusion direction. The dimension parameters a and b shown in Figure 26 characterize the volume fractions ϕ_{ds} and ϕ_{dp} for the system. These quantities are related to a and b by $\phi_{ds} = a^3$ and $\phi_{dp} = b^2$. The effective permeability of the system defined by Figures 25 and 26 can be obtained following a derivation similar to the ones used above by summing up the
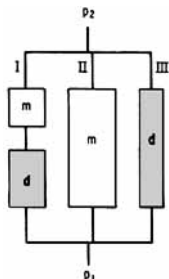

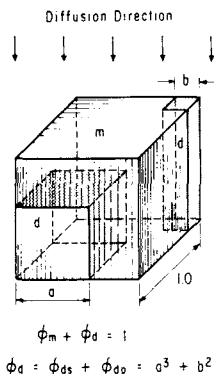Fig. 25. Diffusional resistance combination according to model 3 for drawn Korad behavior.

Fig. 26.   Three-dimensional representation of model 3, describing the morphology of drawn Korad following the approach of Nielson.[31] ϕ_{dp} and ϕ_{ds} are the d-phase volume fractions of the system exhibiting parallel and series diffusion character, respectively.

diffusive flows over branches I, II, and III of Figure 25 given below:

$$\text{I:}\quad \frac{P_{\mathrm{I}}A_{\mathrm{I}}}{l_{\mathrm{I}}} = \left[\frac{(1-a)}{P_m a^2} + \frac{a}{P_d a^2}\right]^{-1} \tag{25}$$

$$\text{II:}\quad \frac{P_{\mathrm{II}}A_{\mathrm{II}}}{l_{\mathrm{II}}} = P_m(1 - a^2 - b^2) \tag{26}$$

$$\text{III:}\quad \frac{P_{\mathrm{III}}A_{\mathrm{III}}}{l_{\mathrm{III}}} = P_d b^2 \tag{27}$$

Total (I + II + III): $P =$

$$a^2\left[\frac{(1-a)}{P_m} + \frac{a}{P_d}\right]^{-1} + P_m(1 - a^2 - b^2) + P_d b^2 \tag{28}$$

which yields the effective permeability expression for the composite at any given draw ratio as

$$P_\lambda = \phi_{ds}^{2/3}\left[\frac{(1 - \phi_{ds}^{1/3})}{P_m} + \frac{\phi_{ds}^{1/3}}{P_d}\right]^{-1} + P_m(1 - \phi_{ds}^{2/3}) + (P_d - P_m)\phi_{dp} \tag{29}$$

In the case where $\phi_{dp} = 0$, eq. (29) reduces to eq. (10) for P_1 as expected.

By virtue of the last term in eq. (29), model 3 discussed above predicts an essentially linear dependence on ϕ_{dp}. The term $(P_d - P_m)$ is a positive quantity whose magnitude depends strongly on the molecular nature of the penetrant as evident from Tables V and VII. The magnitude of P_d relative to P_m increases rapidly according to the order He $<$ N$_2$ $<$ Ar $<$ CH$_4$. The relative permeability according to the model can be written using eqs. (10) and (29) as

$$\frac{P_\lambda}{P_1} = \left\{\phi_{ds}^{2/3}\left[\frac{(1 - \phi_{ds}^{1/3})}{P_m} + \frac{\phi_{ds}^{1/3}}{P_d}\right]^{-1} + P_m(1 - \phi_{ds}^{2/3}) + (P_d - P_m)\phi_{dp}\right\}$$
$$\times \left\{\phi_d^{2/3}\left[\frac{(1 - \phi_d^{1/3})}{P_m} + \frac{\phi_d^{1/3}}{P_d}\right]^{-1} + P_m(1 - \phi_d^{2/3})\right\}^{-1} \tag{30}$$

and is plotted in Figure 27 for the four gases studied against the quantity ϕ_{dp}/ϕ_d, representing ϕ_{dp} as the fraction of the entire d phase which behaves in a purely parallel mode. The curves drawn in Figure 27 representing the P calculations for model 3 are all straight lines. The ϕ_{ds} terms in eq. (30) contribute a very small nonlinear character to the P_λ/P_1 curves; however, this effect is not noticeable as it is overshadowed by the much larger ϕ_{dp} term which imparts the linear character to the P_λ/P_1 vs. ϕ_{dp}/ϕ_d curves. All the lines go through $P_\lambda/P_1 = 1.0$ at $\phi_{dp}/\phi_d = 0$, which corresponds to the undrawn material, as expected. The increases in P_λ/P_1 shown in Figure 27 appear to be very much in agreement with the range and relative magnitude of the P/P_0 changes observed experimentally. At $\phi_{dp}/\phi_d = 0.22$, for example, P_λ/P_1 for CH_4 is about 9.3 and those for Ar and N_2 are about 3.8, while the value for He is less than 1.1. The experimental values of P/P_0 for Korad Film drawn to 2.0X at 70°C are quite close to the calculated values as can be seen from Figure 10. A maximum parallel contribution of 20–25% of the total d phase is reasonable since phase inversion in the ordinary sense is very difficult to achieve due to the crosslinking of the PBA.[32]

Unfortunately, there is no readily available means for relating ϕ_{dp} to λ independently. The P_λ/P_1 behavior of Figure 27 coupled with the P/P_0 response to λ shown in Figure 5 suggests that ϕ_{dp} increases for low draw ratios ($\lambda = 1$–2) and sharply levels off for $\lambda > 2$. The morphological transition is probably related to the amount of strain imposed on the system at the molecular level. This would explain the drawing temperature dependence of the permeability response for $\lambda = 2$. It must be remembered that superimposed on the morphological change causing the permeability increases is a likely reduction in the intrinsic permeability of the matrix phase judging from past experience with other glassy polymers.[1-5] This effect, however, is expected to be small compared to the several-fold increase in P observed in the range of low λ values, where the morphological effect is dominant. It probably accounts, however, for the slight decline in P/P_0 for $\lambda > 2$ noted in Figure 5. There, the morphology of the system has attained its maximum conversion. Using Figure 10 in conjunction with the model curves of Figure 27, the fraction ϕ_{dp}/ϕ_d for the system was calculated
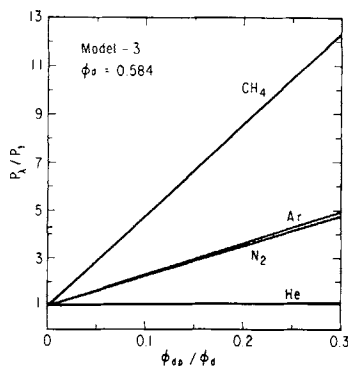

Fig. 27.   Relative permeability P_λ/P_1 as predicted by model 3 plotted against ϕ_{dp}/ϕ_d, the fraction of the d phase exhibiting a parallel diffusion character.

and plotted in Figure 28 against drawing temperature. The dependence of ϕ_{dp}/ϕ_d on drawing temperature reflects both the correlation with the state of orientation in the polymer and the degree of transformation of the rubbery phase from a dispersed to a somewhat continuous morphology with respect to the diffusion direction. This dependence seems reasonable since at temperatures above the matrix T_g the stresses acting to press the rubbery particles together and thereby to increase their area of contact (which relates to the fraction of parallel character) will be considerably lower than below the matrix T_g.

Mechanical and Thermal Behavior

In Figure 29 the storage modulus and tan δ curves for Korad are shown to illustrate the effect of low temperature drawing on these quantities. The solid lines are for a 1.0X sample (i.e., annealed at 70°C). The 1.0X results are essentially identical to those for the as-received film. It shows three transitions which may correspond to the three phases present. The onset of the transitions are located at approximately −50, 30, and 100°C for the PBA, BA/MMA copolymer, and the matrix, respectively. For the drawn (2.0X) sample, the tan δ curve exhibits markedly lowered peaks for all three T_g's, indicative of weaker transitions due to orientation. The storage modulus curves reveal an interesting feature upon comparison. The modulus of the drawn film is higher than that of the undrawn film at low temperatures, but as the T_g of the copolymer is traversed, E' for the 2.0X sample takes a sharp downturn with increasing temperature, becoming significantly lower than that of the undrawn film (1.0X) at high temperatures. This sizeable reduction in E' at high temperatures can be explained on the basis of a morphological change from the dispersed noninteracting original configuration for the rubbery phase into one characterized by some parallel character of both the glassy and rubbery phases. This would be expected to yield a lower modulus compared to the original case because the rubbery elements can accommodate much higher levels of strain for the same stress than those of the glassy regions. This feature is absent in the E' curve of Figure 30 for the sample drawn to 2.0X at 130°C, in agreement with the deformation model described for high temperature and the transport and
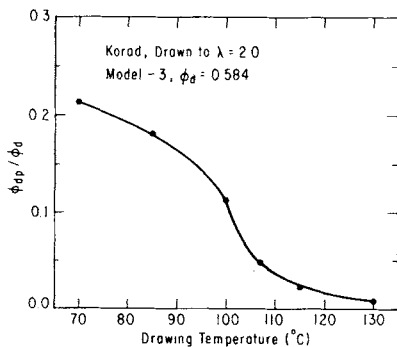

Fig. 28. ϕ_{dp}/ϕ_d plotted against the drawing temperature for λ = 2.0 on the basis of permeability results of Figure 10.
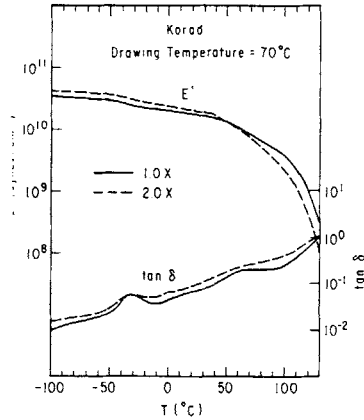
Fig. 29. Storage modulus E' and loss tangent, tan δ, curves for Korad films drawn (2.0X) (- - -) and annealed (1.0X) (- - - -) at 70°C.

thermal shrinkage measurements. However, E' for the 2.0X sample is higher than that for the 1.0X sample by about the same amount observed in Figure 29. This suggests that some orientation is still present in the glassy matrix phase of the polymer for these samples. The tan δ curves for the 130°C samples differ from those of the 70°C samples in that the transitions for the drawn and undrawn films lie closer together on the temperature scale particularly for the two upper transitions. In Figure 31 curves for both drawn samples are superimposed for comparison. The 70°C sample, again, appears to differ from its 130°C counterpart mainly in the high temperature E' response described above. The tan δ peaks for the 70°C sample are also flatter, indicating a higher degree of orientation for all three phases.

The mechanical properties depicted in Figure 32 as a function of drawing temperature provide additional information about the state of orientation in the polymer. The percent elongation at break, shown in the upper plot, is very useful in this regard. It is well known that introducing orientation
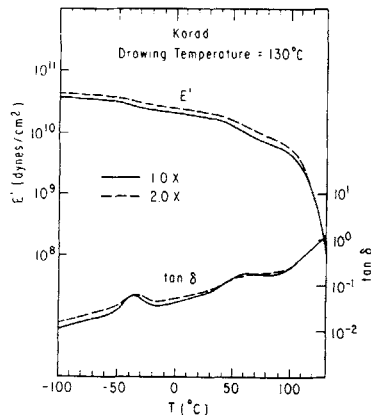

Fig. 30. E' and tan δ curves for Korad films drawn (2.0X) (- - -) and annealed (1.0X) (- - - - -) at 130°C.
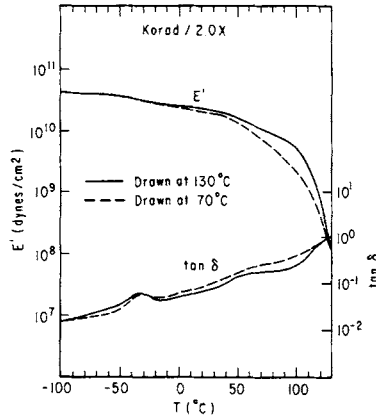
Fig. 31. Comparison of E' and tan δ curves for Korad films drawn at 70 (- - -) and 130°C (----). $\lambda = 2.0$.

into a polymer often causes less ductile tensile behavior, which is manifested as a lower percent elongation. This is due to the originally higher level of strain in the oriented material. The percent elongation curve of Figure 24 exhibits a transition from a low plateau value for low drawing temperatures to a high plateau close to that of the as-received material. This occurs over a short temperature range above the T_g of the matrix (100–110°C). This parallels the permeation results of Figure 10 and other characterization measurements. At a draw ratio of 2.0, the elastic modulus is only modestly increased over the as-received value. However, it is interesting that the modulus increases with increasing drawing temperature, leveling off for temperatures above 100°C. In fact, the modulus for the film drawn at 75°C was slightly below that of the as-received film. This behavior is consistent with the notion that at low drawing temperatures the rubbery phase assumes a more continuous morphological character within the composite,
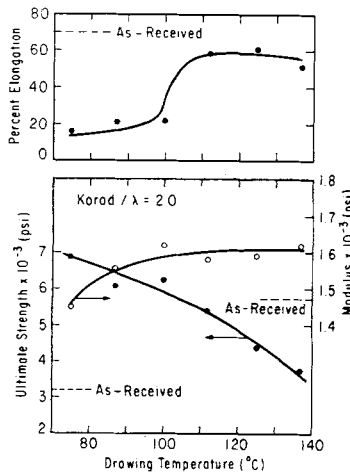

Fig. 32. Percent elongation, ultimate strength, and Young's modulus for drawn Korad films ($\lambda = 2.0$) vs. drawing temperature.

which is the issue believed to cause the observed gas transport behavior. The ultimate strength declines essentially monotonically with drawing temperature, approaching the as-received value for drawing temperatures of 140°C. The ultimate strength behavior is linked to the stress–strain response of the system in the post-yield region. There is marked strain hardening in the case of low temperature drawing. The strain-hardening effect becomes progressively smaller in magnitude with increasing drawing temperature, is absent at about 112°C, and reverses into strain softening for higher temperatures, as was the case for the as-received sample. This behavior is sketched qualitatively in Figure 33. It should also be noted that films drawn at temperatures below 100°C did not show a distinct yield point in their stress–strain diagrams.

Thermal analysis data obtained for drawn and undrawn Korad samples, in the form of DSC thermograms, are shown in Figures 34–36. They correspond to three drawing states: room temperature, 75, and 130°C. In each figure, curves designated I and II correspond to the drawn and undrawn sample thermograms, respectively. All curves have been normalized to a unit mass basis for comparison. The digital subtraction is shown in each figure for better comparison between the two samples. For room-temperature drawing (Fig. 34), the subtraction curve exhibits a negative deviation from the reference line, indicating a smaller overall ΔC_p in the transition of the drawn film. This effect was also noted in connection with orientation of PVC[2] and implies the presence of molecular orientation in both the rubbery (copolymer) and glassy phases. For the opposite case of drawing at elevated temperatures, Figure 36 shows no such negative dip in the difference curve until temperatures exceeding 110°C are reached. In fact, a positive difference is evident over most of the temperature range. Thus, for high temperature drawing only the matrix phase possesses some orientation, which accounts for the observed reduction in C_p at high temperatures. For the film drawn at 75°C (Fig. 35), behavior intermediate between what is seen in Figs. 34 and 36 is observed for the difference curve.

Since annealing oriented polymers near or above T_g is known to reduce the amount of orientation present in a polymer, it was useful to monitor the nature and magnitude of change in P accompanying the annealing of Korad film. In Figure 37, P/P_0 for CH_4 in film drawn to $\lambda = 2.0$ at 70°C is plotted as a function of the annealing temperature. Annealing time for all samples was 10 min and was carried out in the Instron thermal bath under constant strain. In the sub-T_g region, P/P_0 declines in a monotonic
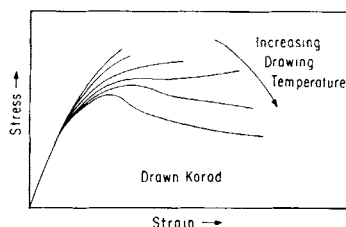

Fig. 33.　Qualitative plot showing changes in the stress–strain response of drawn Korad with increasing drawing temperature.
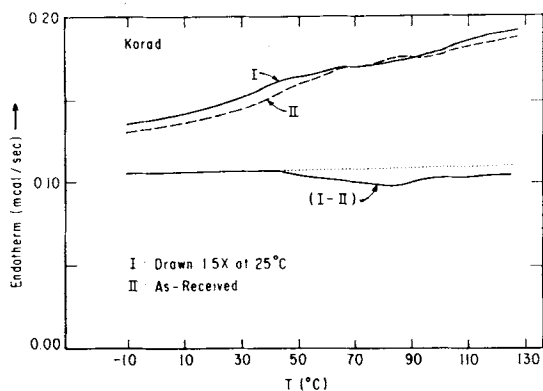
Fig. 34.   Normalized DSC scans and subtraction for as-received (II) and room-temperature (25°C) drawn (1.5X) (I) Korad showing the effect of drawing on endothermic behavior.
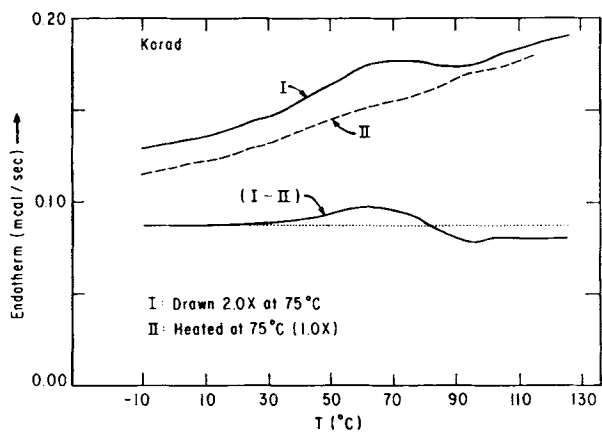

Fig. 35.   Normalized DSC scans and subtraction for Korad films drawn (2.0X) (I) and annealed (1.0X) (II) at 75°C.
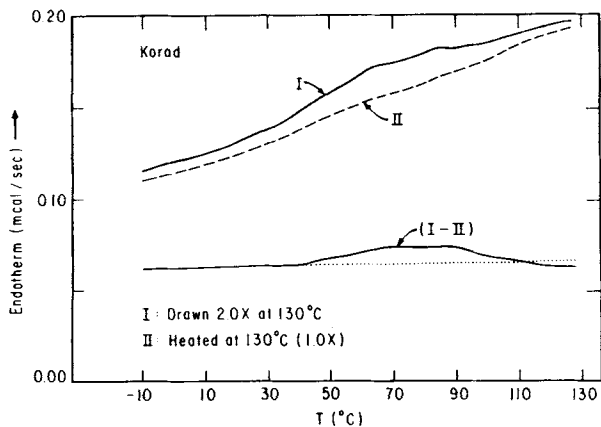

Fig. 36.   Normalized DSC scans and subtraction for Korad films drawn (2.0X) (I) and annealed (1.0X) (II) at 130°C.
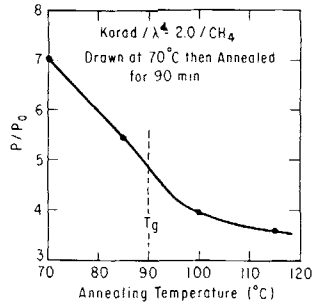
Fig. 37. Effect of annealing temperature on relative permeability, P/P_0, of drawn Korad (λ = 2.0 at 70°C) to CH_4 at 35°C.

fashion with annealing temperature but levels rather abruptly to a plateau beyond 110°C. The reduction is quite substantial for an annealing temperature of 115°C bringing P/P_0 to about 40% of the original value prior to annealing. A permeability reduction is to be expected if the annealing process involves a partial recovery of the original morphological state in the polymer. Upon annealing, the mobility of the matrix phase is enhanced to a level commensurate with the annealing temperature. This allows the matrix to partly relieve the strain originally frozen into it following drawing, thereby reducing the stresses pressing the rubbery particles together. This stress–relaxation process causes the composite as a whole to assume a morphology which is more similar to that of the original film. The permeation behavior observed with drawing is, as a result, reversed by the described morphological recovery of the system. The annealing process is also time-dependent in that the degree of relaxation approaches the equilibrium state according to an exponential decay with respect to time. This time dependent relaxation is reflected in the permeation behavior as shown graphically in Figure 38.

CONCLUSIONS

In this study, the effects of orientation and strain on the gas transport characteristics of a multiphase acrylic emulsion polymer were investigated after subjecting the polymer to mechanical drawing over a wide range of temperatures. Drawing at temperatures below or near the T_g of the glassy
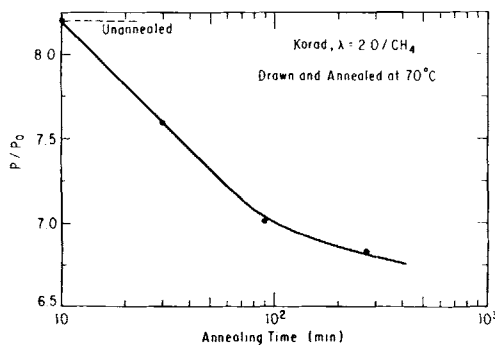

Fig. 38. Effect of annealing time for constant annealing temperature of 70°C on P/P_0 of drawn Korad (λ = 2.0 at 70°C) to CH_4 at 35°C.

matrix phase produced dramatic increases (up to eightfold) in the gas permeability. The permeability increases were accompanied by great losses in the permselectivity of the polymer to various gas pairs. The changes in P were found to strongly depend on the drawing temperature and the molecular diameter of the penetrant gas; P increases were substantially more pronounced when drawing was performed below the T_g of the matrix phase (90°C) compared with drawing about 20°C or more above the T_g, where the permeability increases gradually disappeared. The P increases are larger the greater the molecular diameter of the penetrant. For He, no significant changes in P were noted, whereas the greatest increase in P was observed for CH_4. The apparent diffusion activation energies and preexponential factors for the system were found to decrease for drawn Korad whenever increases in permeability were observed. However, the density of the polymer was unaffected by drawing regardless of the drawing temperature employed.

The permeability response to orientation is believed to arise from a morphological change in the glassy and rubbery phases of the polymer which tremendously increases the contribution of the rubbery phases to the overall permeation behavior of the composite. In the original undrawn Korad, the rubbery component of the polymer is embedded within the glassy matrix by virtue of the shell/core nature of the emulsion polymerization process. This leads to a dispersed noninteractive character for the rubber component and to a diffusion behavior that is predominantly controlled by the permeation characteristics of the continuous matrix phase, which is in a glassy state. The permeation behavior for this system was modeled in this work following the Takayanagi treatment for composites with a single continuous phase. As the polymer is subjected to drawing at low to moderate temperatures, it is believed that the strain induced into the system alters the original morphology of the material, causing the rubbery particles to contact each other forming a morphology comprised essentially of two continuous phases which thereby emphasizes the transport properties of the rubbery component to a greater extent. This translates, in the case of most gases into substantial increases in the permeability as the P values for rubbers are almost invariably much higher than those of glassy polymers. The composite permeability of the new modified morphology was modeled using a treatment based on Nielsen's extension of the Takayanagi model.[31] At temperatures of 110°C or above, the described morphological transformation apparently does not occur to a significant extent upon drawing, even though some orientation is still introduced into the system, particularly in the matrix phase.

Annealing drawn Korad films near or above 90°C at constant strain was found to return the permeability of the system nearly to the original level prior to drawing, thus reversing the effect of drawing. This phenomenon was found to adhere to a time and temperature dependence expected for the kinetics of a thermal relaxation process.

Perhaps the most important finding of this investigation is that, with regard to gas transport behavior, drawing a rubber modified composite can produce property changes which differ fundamentally from those known for homogeneous polymer systems. In the latter case, molecular orientation has been associated with increased barrier characteristics for the material

whereas in the former, as this study has demonstrated, it can cause drastic increases in gas permeability. Thus, generalizations about transport in homogeneous polymers must be applied with caution for heterogeneous polymer systems.

References

1. L. H. Wang and R. S. Porter, *J. Polym. Sci., Polym. Phys. Ed.*, **22**, 1645 (1984).
2. M. J. El-Hibri and D. R. Paul, *J. Appl. Polym. Sci.*, **30**, 3649 (1985).
3. R. E. Barker, R. C. Tsai and R. A. Willency, *J. Polym. Sci., Polym. Symp. Ed.*, **63**, 109 (1978).
4. Y. Ito, *Kobunshi Kagaku*, **19**, 412 (1962).
5. T. E. Brady, S. A. Jabarin, and G. W. Miller, in *Permeability of Plastic Films and Coatings to Gases, Vapors and Liquids*, H. B. Hopfenberg, Ed., Plenum, New York, 1974, pp. 301–320.
6. U.S. Pat. 3,562,235 (1971).
7. D. W. Van Krevelen, *Properties of Polymers*, 2nd ed., Elsevier, Amsterdam, 1976, p. 574.
8. F. W. Billmeyer, Jr., *Textbook of Polymer Science*, 2nd ed., Wiley-Interscience, New York, 1971, p. 504.
9. W. J. Koros, D. R. Paul, and A. A. Rocha, *J. Polym. Sci., Polym. Phys. Ed.*, **14**, 187 (1976).
10. W. J. Koros and D. R. Paul, *J. Polym. Sci., Polym. Phys. Ed.*, **14**, 1903 (1976).
11. W. J. Koros, D. R. Paul, M. Fujii, H. B. Hopfenberg, and V. Stannett, *J. Appl. Polym. Sci.*, **21**, 2899 (1977).
12. J. S. Chiou, J. W. Barlow, and D. R. Paul, *J. Appl. Polym. Sci.*, **30**, 1173 (1985).
13. W. J. Koros, A. H. Chan, and D. R. Paul, *J. Membr. Sci.*, **2**, 165 (1977).
14. D. R. Paul, *Ber. Bunsenges. Phys. Chem.*, **83**, 294 (1979).
15. A. H. Chan and D. R. Paul, *Polym. Eng. Sci.*, **20**, 87 (1980).
16. D. R. Paul, *J. Membr. Sci.*, **18**, 75 (1984).
17. J. S. Chiou and D. R. Paul, *J. Appl. Polym. Sci.*, to appear.
18. P. Masi, D. R. Paul, and J. W. Barlow, *J. Polym. Sci., Polym. Phys. Ed.*, **20**, 15 (1982).
19. A. J. Erb and D. R. Paul, *J. Membr. Sci.*, **8**, 11 (1981).
20. K. Toi, G. Morel and D. R. Paul, *J. Appl. Polym. Sci.*, **27**, 2997 (1982).
21. A. S. Michaels and H. J. Bixler, *J. Polym. Sci.*, **50**, 393 (1961).
22. M. J. El-Hibri and D. R. Paul, to appear.
23. D. R. Paul and W. J. Koros, *J. Polym. Sci., Polym. Phys. Ed.*, **14**, 675 (1976).
24. W. H. Mazur and M. C. Chan, *Chem. Eng. Prog.*, **78**, 38 (1982).
25. K. H. Hellwege, J. Hennig, and W. Knappe, *Kolloid Z.-Z. Polym.*, **188**, 121 (1963).
26. B. R. Bird, W. E. Stewart, and E. N. Lightfoot, *Transport Phenomena*, Wiley, New York, 1960, pp. 744–745.
27. M. Takayanagi, S. Uemura, and S. Minami, *J. Polym. Sci., Part C*, **5**, 113 (1964).
28. T. Okamoto and M. Takayanagi, *J. Polym. Sci., Part C*, **9**, 597 (1968).
29. G. Kraus, K. W. Rollmann, and J. T. Gruver, *Macromolecules*, **3**, 92 (1970).
30. K. Marcincin, A. Romanov, and V. Pollak, *J. Appl. Polym. Sci.*, **16**, 2239 (1972).
31. L. E. Nielson, *J. Appl. Polym. Sci.*, **21**, 1579 (1977).
32. R. A. Dickie, M.-F. Cheung, and S. Newman, *J. Appl. Polym. Sci.*, **17**, 65 (1973).